Sulfated RaxX, which represents an unclassified group of ribosomally synthesized post-translationally modified peptides, binds a host immune receptor

Dee Dee Luu[1,8], Anna Joe[1,2,8], Yan Chen[3], Katarzyna Parys[4], Ofir Bahar[1,5], Rory Pruitt[1,6], Leanne Jade G. Chen[3], Christopher J. Petzold[3], Kelsey Long[1], Clifford Adamchak[1], Valley Stewart[7], Youssef Belkhadir[4], Pamela C. Ronald[1,2,9,*]

[1]Department of Plant Pathology and the Genome Center, University of California, Davis, CA 95616, USA

[2]Feedstocks Division, Joint Bioenergy Institute, Emeryville, CA 94608, USA

[3]Technology Division, Joint Bioenergy Institute, Emeryville, CA 94608, USA

[4]Gregor Mendel Institute, Austrian Academy of Sciences, Vienna Biocenter, Dr Bohr Gasse 3, Vienna, Austria

[5]Present address: Department of Plant Pathology and Weed Research, Agricultural Research Organization, Volcani Center, Rishon LeZion, Israel

[6]Present address: Department of Plant Biochemistry, University of Tübingen, D-72076 Tübingen, Germany

[7]Department of Microbiology & Molecular Genetics, University of California, Davis, CA 95616, USA

[8]These authors contributed equally

[9]Lead contact

*Correspondence: pcronald@ucdavis.edu

ABSTRACT

The rice immune receptor XA21 is activated by the sulfated microbial peptide RaxX (required for activation of XA21-mediated immunity X) produced by *Xanthomonas oryzae* pv. *oryzae* (*Xoo*). Mutational studies and targeted proteomics revealed that RaxX is processed and secreted by the protease/transporter RaxB, whose function can be partially fulfilled by a noncognate peptidase-containing transporter B (PctB). RaxX is cleaved at a Gly-Gly motif, yielding a mature peptide that retains the necessary elements for RaxX function as an immunogen and host peptide hormone mimic. These results indicate that RaxX is a founding member of a previously unclassified and understudied group of tyrosine sulfated RiPPs (ribosomally synthesized, post-translationally modified peptides). We further demonstrate that sulfated RaxX directly binds XA21 with high affinity. This work reveals a complete, previously uncharacterized biological process: bacterial RiPP biosynthesis, secretion, binding to a eukaryotic receptor and triggering of a robust host immune response.

INTRODUCTION

Ribosomally synthesized and post-translationally modified peptides (RiPPs) include anti-microbial, anti-cancer, insecticidal, and quorum sensing peptides (Arnison et al., 2013). RiPPs are structurally and functionally diverse yet share commonalities. They are ribosomally synthesized as a precursor peptide with a cleavable N-terminal leader and a post-translationally modified core that becomes the final secreted bioactive RiPP (Figure 1A; Arnison et al., 2013). Many RiPP leaders direct the modification and/or

export proteins to the core. This permits the biosynthetic proteins to act on a diverse range of core peptides while maintaining substrate specificity (Oman and van der Donk, 2010) and allows for leader peptide-guided designed synthesis of hybrid RiPPs (Burkhart et al., 2017).

RiPPs achieve substantial chemical diversity through extensive post-translational modifications and are divided into over 20 groups (Arnison et al., 2013). One group that has not been well-studied nor formally categorized as RiPPs are tyrosine sulfated peptides.

Tyrosine sulfation is a post-translational modification that influences receptor-ligand binding in diverse host-microbe interactions (Stone et al., 2009). For example, in humans, tyrosine sulfation of the integral membrane protein CCR5 (C-C chemokine receptor type 5) significantly enhances binding of the human immunodeficiency virus (HIV) envelope glycoprotein, facilitating HIV entry (Farzan et al., 1999).

In rice, the transmembrane immune receptor XA21, which shares similarities to animal TOLL like receptors (TLRs) and the *Arabidopsis* flagellin-sensitive 2 (FLS2) and EF-Tu receptors (EFR) (Dardick et al., 2012), responds to sulfated derivatives of the microbial peptide RaxX (required for activation of XA21-mediated immunity X) produced by the Gram-negative pathogenic bacterium *Xanthomonas oryzae* pv. *oryzae* (*Xoo*) (Pruitt et al., 2015, 2017; Schwessinger et al., 2016; Wei et al., 2016). Tyrosine sulfated RaxX16, a 16-residue synthetic peptide derived from residues 40-55 of the 60-residue RaxX precursor, is the shortest characterized immunogenic derivative of RaxX (Pruitt et al., 2017). RaxX16 shares a 13-residue sequence with high similarity to the 18-residue plant peptide hormone PSY1 (plant peptide containing sulfated tyrosine; Pruitt et al.,

2017). PSY1 promotes cellular proliferation and expansion *in planta* (Amano et al., 2007) and increases root growth in both *Arabidopsis* and rice (Pruitt et al., 2017). Exogenous application of sulfated RaxX16 also promotes root growth (Pruitt et al., 2017), which is consistent with the hypothesis that RaxX mimics host PSY1 and PSY1-like proteins. These observations indicate that RaxX16 contains the biologically active domain of RaxX.

In *Arabidopsis*, PSY1 is ribosomally synthesized as a 75-residue precursor peptide and proteolytically processed into the mature secreted 18-residue sulfated and glycosylated peptide (Amano et al., 2007). Based on similarities between PSY1 and RaxX16, we hypothesized that sulfated RaxX is also processed and secreted to produce an extracellular molecule that can interact with host receptors.

The *raxX* gene is adjacent to the *raxSTAB* operon, encoding the RaxST tyrosylprotein sulfotransferase, which catalyzes sulfation of RaxX tyrosine residue 41, and two components of a predicted type I secretion system (T1SS): the RaxA periplasmic adaptor protein and the RaxB peptidase-containing ABC (ATP-binding cassette) transporter (PCAT; Figure 1B; Pruitt et al., 2015; da Silva et al., 2004). In other characterized PCATs, the N-terminal peptidase domain cleaves the substrate leader immediately after a Gly-Gly (GG) motif, and the processed substrate is secreted through the PCAT, periplasmic adaptor protein and TolC, an outer membrane channel protein (Kanonenberg et al., 2013).

Previously, we reported that derivatives of the immunogenic *Xoo* strain PXO99 containing null alleles of *raxX*, *raxST*, or *raxC* (encoding the *Xoo* TolC ortholog) evade XA21-mediated recognition, but strains with null alleles of *raxA* or *raxB* elicit a partial

XA21-mediated immune response (Pruitt et al., 2015; da Silva et al., 2004). These results suggest that RaxA and RaxB are important for RaxX secretion but RaxX can also be released outside the cell independent of *raxA*/*raxB*.

Here, we report that synthetic RaxX peptide directly binds the extracellular domain (ECD) of the XA21 immune receptor ($XA21^{ECD}$), an interaction enhanced by tyrosine sulfation of RaxX. We also demonstrate that RaxB is required for proteolytic processing and secretion of RaxX and identify a second PCAT PctB (peptidase-containing transporter component B) that can partially compensate for deletion of *raxB*. Our genetics and targeted proteomics data indicate that RaxX is ribosomally synthesized as a precursor peptide and cleaved downstream of a GG-motif in a RaxB-dependent manner. This proteolytic event releases the mature RaxX core peptide containing the sulfated Tyr-41 and the minimal 16-residue active region (Figure 1B). These results indicate that RaxX is a tyrosine sulfated RiPP, a previously undescribed class of RiPPs that mediate intercellular interactions.

RESULTS

Sulfated RaxX peptide binds XA21 with high affinity

We previously demonstrated that *in vivo* tyrosine sulfation of RaxX by RaxST is required to activate XA21-dependent immune responses (Pruitt et al., 2015), suggesting that sulfated, but not non-sulfated, RaxX is recognized by XA21. To test if RaxX directly binds to the XA21 immune receptor, we used microscale thermophoresis (MST), an optical tool that analyzes protein and small-molecule interactions (Wienken et al., 2010).

The MST assays were conducted using $XA21^{ECD}$ (XA21 residues 23-649) with varying concentrations of peptide to measure the dissociation constant (K_D). When we titrated a synthetic 21-residue derivative of RaxX (RaxX21; residues 35-55) in the presence of $XA21^{ECD}$, we observed a K_D of 400 nM with the non-sulfated form (RaxX21-nY; Figure 2). This K_D is 20-fold higher than the sulfated form (RaxX21-sY), which had a K_D of 20 nM (Figure 2), indicating that sulfated RaxX binds XA21 with higher affinity than non-sulfated RaxX.

Although RaxX shares similarities with PSY1 in both sequence and root growth-promoting activities, synthetic sulfated PSY1 peptides derived from *Arabidopsis* and rice fail to activate XA21-dependent immune responses (Pruitt et al., 2017). Consistent with these reports, sulfated PSY1 failed to specifically bind $XA21^{ECD}$ (Figure 2). These results indicate that RaxX binding to $XA21^{ECD}$ is a specific interaction, which is enhanced by sulfation.

SRM-MS detects RaxX as a secreted mature peptide

Based on its similarity to PSY1 and its direct binding to $XA21^{ECD}$, we hypothesized that sulfated RaxX interacts with host receptors as a secreted proteolytically processed, mature peptide. To test this hypothesis, we assessed the presence of secreted RaxX in the extracellular milieu. Secreted proteins were harvested from *Xoo* strains grown in plant-mimicking media, concentrated, and digested with trypsin. The predicted mature and non-processed precursor RaxX peptides (represented by the DYPPPGANPK and HVGGGDYPPPGANPK tryptic peptides, respectively) were specifically detected by selected reaction monitoring-mass

spectrometry (SRM-MS), which was calibrated using tryptic digests of RaxX16 (DYPPPGANPKHDPPPR) synthetic peptide and purified recombinant full-length RaxX (RaxX60; Figures 3A, S1A, and S1B).

Similar to previous reports, we detected the RaxX non-processed precursor in the cell lysate (Figure 3B; Pruitt et al., 2015). However, only mature, processed RaxX was detected in the supernatant of the wildtype PXO99 strain (Figure 3). Mature RaxX was not detected in the Δ*raxX* negative control (Figures 3C and 3D), indicating that the observed peaks are specific for RaxX. Because trypsin is not known to cleave after glycine, which precedes the detected DYPPPGANPK tryptic peptide, these results suggest that the RaxX precursor is cleaved by an endogenous *Xoo* protease after Gly-39 and secreted outside the cell as a mature peptide (Figure 1B).

We also attempted immunoblot analysis as a complementary method to detect RaxX. However, an antibody generated against RaxX failed to detect RaxX16 or RaxX from *Xoo* supernatants (Figures S1C and S1D). We therefore used SRM-MS alone in subsequent experiments to verify RaxX secretion.

Sequence analysis identifies a candidate secondary RaxX maturation and secretion system: PctAB

Prokaryotic RiPPs typically encode the maturation and secretion proteins in the same genomic region as the peptide (Figure 1A). We previously demonstrated that a strain carrying a null allele of *raxC*, encoding the predicted T1SS outer membrane protein, fails to activate XA21-mediated immunity, supporting a role for *raxC* in RaxX secretion (da Silva et al., 2004). In contrast, strains carrying null alleles of *raxB* or *raxA*,

encoding the putative RaxX-associated PCAT and periplasmic adaptor proteins, respectively, maintain the ability to partially activate XA21-mediated immunity (da Silva et al., 2004). These results suggest that RaxX can be released in a *raxA*/*raxB*-independent manner.

The RaxB sequence contains an N-terminal C39 peptidase domain characteristic of PCATs (e.g. *Escherichia coli* colicin V (ColV) transporter CvaB), which have dual functionality as both a transporter and protease (Figure 4A; da Silva et al., 2004; Håvarstein et al., 1995; Wu and Tai, 2004). Query of the RaxB C39 peptidase domain sequence in BLAST searches of the PXO99 genome identified only one other candidate PCAT, which shares 50% sequence identity with RaxB (41% identity with *E. coli* CvaB). We named this gene (PXO_RS14825) as *pctB* (Figure 4B).

Immediately upstream of *pctB* is a gene, which we named *pctP* (PXO_RS14830), encoding a putative rhomboid family intramembrane serine protease (Figure 4B) that typically cleaves the transmembrane domain of membrane proteins (Freeman, 2014). Further upstream are an insertion sequence (IS*1112*), a region of uncertain heritage likely derived from multiple insertion and deletion events, and a predicted gene (PXO_RS14840), which we named *pctA,* encoding a putative periplasmic adaptor protein (Figure 4B). PctA shares 32% sequence identity with RaxA (24% identity with *E. coli* CvaA, the adaptor component of the ColV secretion system (Zhang et al., 1995)). Given the close proximity of *pctA* and *pctB* and the absence of other PCAT-encoding genes in the genome, we hypothesized that PctA and PctB form an alternate T1SS that can secrete sufficient levels of sulfated RaxX to activate XA21.

185 **PctB partially compensates for the loss of RaxB**

186 To assess the potential role of PctB in RaxX maturation and secretion, we
187 deleted *raxB* and *pctB* singly or together from the PXO99 genome. The resultant mutant
188 strains (designated Δ*raxB*, Δ*pctB*, and Δ*raxB* Δ*pctB*, respectively*)* were inoculated onto
189 rice plants by clipping leaf tips with scissors dipped in bacterial suspension. Lesion
190 lengths and bacterial densities *in planta* measured 14 days after inoculation were
191 comparable to wildtype PXO99 on Taipei 309 (TP309) rice plants, which lack *Xa21*
192 (Figures 5A and 5C; Song et al., 1995). This indicates that deletion of genes encoding
193 these putative transporters do not directly compromise *Xoo* virulence under the tested
194 conditions.

195 We next tested the effect of the mutant strains on XA21-TP309 rice, a derivative
196 of TP309 that expresses *Xa21* (Song et al., 1995), to assess XA21-dependent
197 responses. As previously reported, XA21-TP309 rice were resistant to PXO99 infection
198 and had short lesions (<5 cm) and low bacterial densities (6.8 x 10^6 CFU/leaf) *in planta*
199 (Figures 5A-5C; Song et al., 1995). We observed that the Δ*raxB* mutant formed short (<
200 5 cm) to intermediate (6-9 cm) lesions on XA21-TP309, which varied between
201 experiments, but the Δ*pctB* mutant consistently formed short (<5 cm) lesions similar to
202 PXO99 (Figures 5A and 5B). Both Δ*raxB* and Δ*pctB* single mutants accumulated to
203 populations of ~4.5 x 10^7 CFU/leaf, roughly 6.6-fold higher than PXO99 (Figure 5C). In
204 contrast, the Δ*raxB* Δ*pctB* double mutant formed long lesions (>14 cm) and
205 accumulated to 8.4 x 10^8 CFU/leaf, over 4- and 120-fold higher than the PXO99
206 population, respectively (Figures 5A-5C). These phenotypes were comparable to the
207 Δ*raxX* control (Figures 5A and 5C). Similarly, the Δ*raxA* Δ*pctA* double mutant,

containing mutations in genes for the predicted periplasmic adaptor proteins RaxA and PctA, formed longer lesions than the Δ*raxA* and Δ*pctA* single mutants (Figure S2). Collectively, these results suggest that sulfated RaxX is not secreted in both the Δ*raxA* Δ*pctA* and Δ*raxB* Δ*pctB* double mutants, allowing these strains to evade XA21. These results also suggest that PctA and PctB can partially compensate for the loss of RaxA and RaxB, respectively.

RaxB is the primary PCAT required for RaxX maturation and secretion

The Δ*raxB* Δ*pctB* double mutant accumulates to high population levels in XA21-TP309 plants (Figure 5C), indicating that this strain can evade detection by the XA21 immune receptor. This result supports the hypothesis that these PCATs secrete sulfated RaxX. Given that *raxB* is genetically clustered with *raxX* (Figure 4A), we hypothesized that RaxB functions as the primary transporter of RaxX and is sufficient to activate XA21 in the absence of PctB. To test this hypothesis, we complemented the Δ*raxB* Δ*pctB* double mutant with p*raxSTAB*, a broad host range vector expressing the entire *raxSTAB* operon with the presumptive native promoter. On XA21-TP309, the p*raxSTAB* plasmid restored *raxB* gene expression as well as activation of XA21-mediated immunity, resulting in short lesions and bacterial densities comparable to wildtype PXO99 (Figures S3A, 5A and 5C). Similarly, p*raxSTAB* restored the ability of the Δ*raxA* Δ*pctA* double mutant to activate XA21-mediated immunity (Figure S2). These results suggest that the RaxAB system is sufficient to secrete RaxX and activate XA21 in the absence of the PctAB system.

As a control, we also expressed p*raxSTAB* in the wildtype PXO99 background. We observed no significant alterations on lesion development with the addition of p*raxSTAB* (Figure S2), suggesting that overexpression of *raxSTAB* did not directly contribute to enhanced activation of the XA21-mediated immune response.

We next assessed, using SRM-MS, if mature RaxX was secreted in the Δ*raxB* Δ*pctB* double mutant. RaxX was detected in the supernatant of the Δ*raxB* Δ*pctB* double mutant only in the presence of the p*raxSTAB* plasmid (Figure 5D). We detected SRM transition peaks of mature RaxX in the p*raxSTAB*-containing strain at the same retention time as wildtype PXO99 and the Δ*raxX* mutant complemented with plasmid-expressed *raxX* (p*raxX*) controls, which were collected and analyzed in the same batch (Figure S3B). Together, these results indicate that RaxB is a necessary and sufficient PCAT for RaxX maturation and secretion.

We also tested if PctB is sufficient to restore RaxX secretion in the Δ*raxB* Δ*pctB* double mutant. For this purpose, we transformed the Δ*raxB* Δ*pctB* double mutant with a broad host range vector expressing the *pctPB* cluster with its presumptive native promoter (p*pctPB*). The p*pctPB* plasmid restored *pctB* gene expression but failed to fully restore XA21-mediated recognition of the Δ*raxB* Δ*pctB* double mutant (Figures S3A and 5A). The p*pctPB*-complemented Δ*raxB* Δ*pctB* double mutant still formed intermediate-to-long lesions (~10 cm) roughly 3-fold longer than PXO99 (Figure 5A). This result suggests that PctB alone cannot effectively secrete RaxX to activate XA21-mediated immunity.

RaxB and PctB carry conserved residues characteristic of bifunctional PCATs

PCATs such as *E. coli* CvaB function as both a transporter and a protease (Håvarstein et al., 1995; Wu and Tai, 2004). The peptidase domain of this class of ABC transporters contains 2 conserved motifs: a cysteine (C) motif and histidine (H) motif (Figure 6A; Dirix et al., 2004; Håvarstein et al., 1995). We found that both RaxB and PctB contain sequences that match the conserved C- and H-motifs, including the conserved Cys, His, and Asp residues (Cys-28/12, His-101/85, Asp-117/101 of RaxB/PctB, respectively) predicted to form the active site catalytic triad (Figure 6A; Wu and Tai, 2004; Wu et al., 2012). Additionally, they contain the conserved Gln residue (Gln-22/6 of RaxB/PctB, respectively) proposed to form the oxyanion hole that stabilizes the Cys-His ion pair (Figure 6A; Ménard et al., 1991; Wu et al., 2012). In contrast, ABC transporters that have a degenerate C39-like domain (CLD) with no proteolytic activity, such as the *E. coli* hemolysin transporter HlyB, do not contain the catalytically essential Cys or conserved Gln (Figure 6A; Lecher et al., 2012). The presence of the complete Cys-His-Asp/Asn catalytic triad and conserved oxyanion hole Gln characteristic of bifunctional PCATs is consistent with the hypothesis that RaxB and PctB also possess proteolytic activity to process RaxX.

Mutation of the RaxB peptidase domain catalytic triad impairs RaxX maturation and secretion

We next assessed the role of the RaxB peptidase domain in RaxX maturation. For these experiments, we transformed the Δ*raxB* Δ*pctB* double mutant with a derivative of p*raxSTAB* containing site-directed missense substitutions of the active-site cysteine (Cys-28) or histidine (His-101) of the RaxB peptidase domain. Cys-28 was mutated to

Ser (C28S) and His-101 was mutated to Asp (H101D), which we hypothesized would abolish proteolytic activity by disrupting formation of the predicted Cys-28, His-101, Asp-117 catalytic triad as demonstrated with *E. coli* CvaB (Wu and Tai, 2004).

Expression of the C28S and H101D mutant derivatives impaired p*raxSTAB*-complemention of the Δ*raxB* Δ*pctB* double mutant phenotype on XA21-TP309 but had no affect on the TP309 control plants (Figures 6B-6D). Wildtype p*raxSTAB* fully complemented the Δ*raxB* Δ*pctB* double mutant phenotype on XA21-TP309, resulting in short lesions (<4 cm) and low bacterial densities (3.9×10^7 CFU/leaf). In contrast, expression of the mutated peptidase derivatives of p*raxSTAB* resulted in long lesions (>9 cm) and high bacterial densities (10^8 CFU/leaf) comparable to the strain without plasmid (Figures 6B-6D). These results indicate that the predicted RaxB peptidase domain is catalytically active and necessary to process and secrete biologically active RaxX.

To assess if mature RaxX is secreted into supernatants of the C28S or H101D RaxB peptidase mutants, we carried out SRM-MS analysis. We detected high SRM transition peaks corresponding to mature RaxX in supernatants of the Δ*raxB* Δ*pctB* double mutant strain carrying wildtype p*raxSTAB* (Figure 6E). In contrast, SRM transitions corresponding to mature RaxX were not detected in the Δ*raxB* Δ*pctB* double mutant carrying p*raxSTAB* with either the C28S or H101D mutation (Figure 6E). We also failed to detect SRM transitions corresponding to mature RaxX in the Δ*raxX* negative control and the Δ*raxB* Δ*pctB* double mutant without plasmid (Figures S3B and 6E). The lack of detectable secreted RaxX in the RaxB peptidase mutants supports our

298 inoculation results, providing further evidence that RaxB serves as the RaxX maturation
299 protease.
300
301 **Mutation of the Gly-Gly cleavage site compromises RaxX maturation and**
302 **secretion**
303 The RiPP precursor typically carries a cleavable N-terminal leader that is
304 removed by a protease (Figure 1A). PCATs cleave the N-terminal leader of substrates
305 downstream of a GG-motif, which contains Gly-Gly or Gly-Ala immediately preceding
306 the cleavage site (Håvarstein et al., 1994, 1995). Based on the observation that key
307 residues in the RaxB catalytic peptidase domain are required for RaxX secretion (Figure
308 6), we hypothesized that RaxX contains an N-terminal GG-motif that is removed by
309 RaxB. In support of this hypothesis, our SRM-MS analysis indicated that the N-terminal
310 39 residues of RaxX are removed prior to secretion (Figure 3). We noted that this leader
311 peptide ends with three conserved glycines and contains conserved hydrophobic
312 residues at positions -4, -7, -12, and -15 distal to the cleavage site, a pattern typical of
313 PCAT substrates and necessary for interaction with the peptidase (Figures 3A, 7A and
314 S4A; Aucher et al., 2005; Kotake et al., 2008). These observations suggest that the
315 predicted RaxX leader resembles the leader of GG-motif-containing peptides typically
316 processed and secreted by PCATs.
317 Studies of the peptide mesentericin Y105 (MesY) produced by *Leuconostoc*
318 *mesenteroides* indicate that the GG-motif preceding the MesY cleavage site is critical
319 for efficient processing and secretion (Aucher et al., 2005). Based on this observation,
320 we hypothesized that the GG-motif in the predicted RaxX leader sequence is critical for

RaxB-mediated processing of RaxX. To test this hypothesis, we generated site-directed missense substitutions of the conserved glycine residues (37-39) preceding the cleavage site of RaxX. As Aucher et al. (2005) demonstrated that secretion of MesY was significantly reduced or completely abolished when Gly at the -2 position from the cleavage site was mutated to Ala or Asp or when Gly at the -1 position from the cleavage site was mutated to Arg or Asp, we generated homologous missense substitutions of RaxX Gly-(37-39). As a control, we also generated missense substitutions of Gly-Ala pairs further upstream of the cleavage site: Gly-11, Ala-12 and Gly-20, Ala-21. These mutant variants of RaxX were expressed as derivatives of the p*raxX* plasmid in the Δ*raxX* mutant background.

The resulting mutants were inoculated onto rice plants. These mutants formed long (>12 cm) lesions comparable to PXO99 on the TP309 control plants (Figures 7B, S4B, and S4C). On XA21-TP309, Δ*raxX* formed long lesions (>15 cm) and this phenotype was complemented to short lesions by p*raxX* as previously reported (Figures 7B, S4B, and S4C; Pruitt et al., 2015). Similarly, p*raxX* derivatives containing mutations in RaxX residues Gly-11, Ala-12, Gly-20, or Ala-21 still complemented the Δ*raxX* mutant phenotype (Figures S4B and S4C). This result suggests that these residues are not necessary for processing nor secretion of RaxX. In contrast, p*raxX* derivatives containing mutations in Gly-(37-39) were impaired in their ability to complement the Δ*raxX* mutant phenotype (Figures 7B, S4B, and S4C). Expression of the G37D and G38A derivatives resulted in intermediate lesions (11-12 cm) but the G38D, G38R, and G39D derivatives resulted in long lesions (>15 cm) similar to the Δ*raxX* mutant without plasmid control (Figures 7B, S4B, and S4C). Bacterial densities were also comparable

among the Δ*raxX* mutant and the G38D and G39D-expressing strains (Figure 7C). These results suggest that Gly-(37-39), which immediately precede the cleavage site, are essential for RaxX maturation and/or secretion.

We next assessed if we could detect secreted RaxX in supernatants of *Xoo* strains carrying mutations in the leader peptide. We did not detect SRM transitions of RaxX above background levels in supernatants of the Δ*raxX* mutant carrying the G38D and G39D derivatives (Figure 7D), suggesting that RaxX is neither processed nor secreted when Gly-38 or Gly-39 is mutated to Asp. In contrast, we detected RaxX in supernatants of the Δ*raxX* mutant carrying the G37D p*raxX* derivative although at reduced levels compared to expression of wildtype p*raxX* (1.5×10^3 vs. 5.8×10^3 total peak area, respectively; Figure 7E). The accumulation of intermediate amounts of RaxX peptide secreted from the G37D mutant strain is consistent with the formation of intermediate lesion lengths on XA21-TP309 plants inoculated with this strain (Figures 7B and 7E). Taken together, our results suggest that proper RaxX maturation and secretion, which require the Gly-38, Gly-39 cleavage site, are necessary steps in the biogenesis of the immunogenic peptide.

DISCUSSION

Tyrosine sulfation of RaxX enhances XA21 binding

RaxX immunogenicity is dependent on sulfation of Tyr-41 (Pruitt et al., 2015). Our MST results demonstrate that this modification increases the affinity of RaxX binding to $XA21^{ECD}$ (Figure 2), resulting in a K_D comparable to the RaxX concentration

367 needed to trigger the half maximal immune response of XA21 (~20 nM) and induce root
368 growth (Pruitt et al., 2015, 2017). Tyrosine sulfation has similarly been observed to
369 enhance interaction of the disulfated pentapeptide phytosulfokine (PSK) with its cognate
370 receptor PSKR1 in *Arabidopsis* and carrot. Based on crystal structure studies, the two
371 sulfate groups on PSK form hydrogen bonds and van der Waals packing with residues
372 on PSKR1 (Wang et al., 2015). This sulfate group-mediated interaction stabilizes
373 PSKR1, which in turn allosterically induces heterodimerization with the SERK (somatic
374 embryogenesis receptor-like kinase) co-receptor, resulting in activation of PSKR1
375 (Wang et al., 2015). Analogous structural studies will provide insights into how sulfation
376 of RaxX Tyr-41 contributes to the RaxX-XA21 interaction.
377
378 **RaxX shares similarities to RiPPs**
379 RaxX is predicted to mimic the activity of the plant peptide hormone PSY1 (Pruitt
380 et al., 2017). Our results indicate that RaxX is ribosomally synthesized as a precursor
381 that is proteolytically processed by RaxB into a mature peptide (Figure 1B). This mature
382 RaxX peptide includes the same residues covered by RaxX16, which is sufficient to
383 activate XA21-mediated immunity and promote root growth in rice (Figure 3A; Pruitt et
384 al., 2017). These residues also precisely overlap the conserved 13-residue region found
385 in mature PSY1 from *Arabidopsis* and in putative PSY-like proteins from various plant
386 species including rice (Amano et al., 2007; Pruitt et al., 2017). Furthermore, the mature
387 RaxX and PSY1 peptides start with the same residues, Asp-Tyr, with the critical sulfated
388 tyrosine at the same position. Mature RaxX therefore intimately resembles host PSY-
389 like proteins.

The small size (<10 kDa), presence of a post-translational modification (sulfated tyrosine in this case), and proteolytic maturation of RaxX and PSY1 are defining characteristics of RiPPs (Arnison et al., 2013). In addition to PSY1, plants produce other secreted tyrosine-sulfated peptides that regulate plant growth including PSK, root meristem growth factor (RFG), and Casparian strip integrity factor (CIF) (Matsubayashi and Sakagami, 1996; Matsuzaki et al., 2010; Doblas et al., 2017; Nakayama et al., 2017). Similar to RaxX and PSY1, PSK, RFG, and CIF are proteolytically processed from larger precursor peptides and secreted. We therefore propose that these peptides be classified as RiPPs.

RiPPs are subdivided into over 20 groups according to their biosynthetic machinery and structural features imparted primarily by the post-translational modification(s) that decorate the core (Arnison et al., 2013). However, more groups continue to be added as new RiPPs are identified. Given the similarities of RaxX, PSY1, PSK, RFG, and CIF, we propose that these peptides be classified as a new group of RiPPs defined by the presence of the sulfated tyrosine.

Does PctB process and secrete other RiPPs?

Our results indicate that RaxAB is the cognate RaxX maturation and secretion system and can be partially complemented by PctAB. This functional redundancy is rather unusual given the low sequence identity shared between the two systems, which are also independently distributed among Xanthomonads. For instance, the *X. albilineans* genome contains *pctAPB* but not *raxX* nor *raxSTAB*, whereas the *X.*

412 *euvesicatoria* genome contains *raxX* and *raxSTAB* but not *pctAPB*. These observations
413 suggest that RaxX is not the cognate substrate for PctB.

414 Because PctB is predicted to have a functional C39 peptidase domain (Figure
415 6A), we hypothesize that its cognate substrate is a GG-motif-containing peptide. Based
416 on the annotated PXO99 sequence (NC_010717.2), two hypothetical genes,
417 PXO_RS14845 and PXO_RS14850 (here referred to as *pct-92* and *pct-75*,
418 respectively), are encoded upstream of *pctA* (Figure 4B). *pct-92* and *pct-75* are
419 predicted to encode 92- and 75-residue peptides, respectively, that contain a GG-like
420 leader of 28 and 19 amino acids, respectively (Figure S4A). If Pct-92 and Pct-75 are
421 both PctB substrates, then this would suggest that PctB can tolerate leaders that vary in
422 sequence and length. Such substrate tolerance has been observed in PCATs such as
423 LagD, HalT, and LicT from *Lactococcus lactis*, *Bacillus halodurans*, and *B. licheniformis*,
424 respectively, which process and transport two cognate peptides that function together
425 as a two-component antimicrobial molecule (Caetano et al., 2014; Håvarstein et al.,
426 1995; Lawton et al., 2007). Because the leader of the two peptide components can vary
427 in sequence and length (Figure S4A), these transporters exhibit a relaxed specificity
428 and sometimes tolerate noncognate substrates (Caetano et al., 2014). This may explain
429 why PctB is able to tolerate RaxX, at least to some extent. However, we have yet to
430 confirm that *pct-92* and *pct-75* encode actual peptides. It is also unclear if these putative
431 peptides are post-translationally modified as no known modification enzymes are
432 encoded in the same genomic region (Figure 4B). Therefore, further studies are needed
433 to analyze these putative PctB substrates and identify essential determinants that allow
434 PctB to distinguish substrates.

435

436 **Does the RaxX leader peptide have functional roles in RiPP biosynthesis other**
437 **than peptidase recognition?**

438 In the RaxX leader peptide, residues proximal to the peptidase cleavage site are
439 well conserved in *raxX* alleles from all *Xanthomonas* species (Figure 7A). This includes
440 Gly-38 and Gly-39 preceding the cleavage site, which are critical for proper RaxX
441 maturation and secretion (Figure 6), as well as the hydrophobic residues that occupy
442 positions -4, -7, and -12 from the cleavage site (Val-36, Trp-33, and Leu-28,
443 respectively), which are proposed to position the Gly-Gly cleavage site in the enzyme's
444 active site (Ishii et al., 2010). These features are also conserved in leaders of PCAT
445 substrates, including RiPPs and unmodified peptides (Figure S4A), suggesting that this
446 region of the RaxX leader is important for recognition by the RaxB and PctB peptidase
447 domain. However, it is unclear if sulfation of RaxX, which occurs one residue from the
448 cleavage site, is required for recognition by RaxB or possibly impairs recognition by
449 PctB.

450 Because many unmodified peptides have a shorter leader peptide, the extended
451 N-terminus of RaxX may have other functional roles aside from maturation and
452 secretion that we have yet to identify.

453 One proposed role of the leader peptide is to keep the precursor inactive during
454 biosynthesis as demonstrated for *Lactococcus lactis* lacticin 481, an antimicrobial RiPP
455 of the lanthipeptide class (Xie et al., 2004). However, the observation that exogenous
456 application of RaxX60, representing the full-length precursor peptide, is able to activate
457 XA21-dependent immune responses (Pruitt et al., 2015) and promote root growth in

458 *Arabidopsis* and rice (unpublished data), does not support a role for the RaxX leader in
459 maintenance of an inactive state.
460 Another possibility is that the leader peptide serves as a recognition motif for
461 post-translational modification enzymes. We previously detected sulfated non-
462 processed RaxX in *Xoo* cell lysates (Pruitt et al., 2015), suggesting that sulfation occurs
463 while the leader is attached. However, under *in vitro* conditions, RaxST can sulfate a
464 peptide derivative of human CCR5, containing only an aspartate preceding the tyrosine
465 (Han et al., 2012). This result suggests that the RaxX leader is not required for RaxST
466 function. Similarly, the lacticin 481 precursor LctA, which is post-translationally modified
467 by dehydration and cyclization reactions catalyzed by LctM, does not require the leader
468 for its modification (Levengood et al., 2007). Instead, the presence of the leader peptide
469 promotes the efficiency of LctM modification of the LctA core peptide even when
470 supplemented *in trans* as a synthetic peptide (Levengood et al., 2007) or covalently
471 fused to LctM (Oman et al., 2012). Further studies are needed to determine if the RaxX
472 leader helps recruit RaxST or enhance its sulfotransferase activity in an analogous
473 manner.
474
475 **Knowledge of RiPP biosynthesis can be used to engineer a diversity of tyrosine**
476 **sulfated molecules**
477 *raxX* is genetically clustered with *raxST*, *raxA* and *raxB*, which are each involved
478 in its biosynthesis. The simplicity of the RaxX biosynthetic machinery makes it an ideal
479 system to study how sulfation affects substrate specificity and activity of the biosynthetic
480 proteins. This information can provide insights into the development of strategies to

engineer new tyrosine sulfated molecules such as hybrid RiPP products. Burkhart et al. (2017) used such an approach to demonstrate that sequences recognized by unrelated RiPP modification enzymes, including thiazoline-forming cyclodehydratases and lanthipeptide synthetases, can be combined into a single chimeric leader within a precursor peptide. Co-expression of this chimeric construct with the appropriate modification enzymes led to the production of hybrid RiPPs *in vivo*. With the addition of leader-independent "tailoring" modification enzymes, the chemical diversity of these hybrid RiPPs can be further extended. We envision that the Rax system can be similarly exploited to increase the chemical diversity and potency of sulfated molecules that may be useful as therapeutic agents to suppress infection or activate the immune response of plants and animals.

Conclusion

Here we show that PCAT processing is required for both the maturation and export of bacterial RaxX, an immunogen that binds a eukaryotic receptor. These results suggest that RaxX is a tyrosine sulfated RiPP, a group not previously described. We further identified and defined the RaxX leader, which contains residues that are critical for its maturation and secretion. These results set the stage for leader peptide-guided biosynthetic strategies to extend the chemical diversity of hybrid RiPPs.

MATERIALS AND METHODS

Peptides

Tyrosine sulfated (sY) and/or nonsulfated (nY) versions of RaxX13 (DYPPPGANPKHDP), RaxX16 (DYPPPGANPKHDPPPR), and RaxX21 (HVGGGDYPPPGANPKHDPPPR) were synthesized. The synthetic peptides were ordered from Pacific Immunology (Ramona, CA), with the exception of RaxX16, which was ordered from Peptide 2.0 (Chantilly, VA). Tyrosine sulfated PSY1 was synthesized by the Protein Chemistry Facility at the Gregor Mendel Institute. All of the peptides were resuspended in ddH_20. Recombinant full-length RaxX (RaxX60-sY and RaxX60-nY) was isolated from an engineered *E. coli* strain using an expanded genetic code approach as previously described (Pruitt et al., 2015).

XA21^{ECD} expression and purification

The extracellular domain (ECD) of XA21 (residues 23 - 649) was amplified using primers listed in Table S2 and inserted into the baculovirus transfer vector pMelBac B1 (Invitrogen, Carlsbad, CA) using RecA-mediated Sequence and Ligation Independent Cloning (SLIC) strategy (Scholz et al., 2013). A C-terminal Strep II-9xHis tag was fused to XA21^{ECD} and verified by Sanger Sequencing. XA21^{ECD} -StrepII-9xHis was produced by secreted expression in baculovirus-infected High Five insect cells, harvested 72 hours post-infection. Subsequently, the protein was affinity purified by Ni-NTA chromatography (Ni Sepharose excel, GE Healthcare, Chicago, IL) and subjected to size-exclusion chromatography column (Superdex 200 16/60, GE Healthcare) pre-equilibrated with 50 mM NaH_2PO_4/Na_2HPO4 pH 7.5, 200 mM NaCl, 5% Glycerol. All of the purification steps were checked by SDS-PAGE.

527 **Microscale thermophoresis (MST)**

528 Purified XA21^{ECD} was labelled with a fluorescent dye using Monolith™ Protein Labelling
529 Kit RED-NHS (Amine Reactive; NanoTemper Technologies, San Francisco, CA).
530 Fluorescently-labelled XA21^{ECD} (at constant concentration 0.0133 μM) was mixed with
531 varying peptide concentrations (ranging from 0.00006 to 2 μM) in buffer containing 50
532 mM NaH_2PO4/Na_2HPO4 pH 7.5, 200 mM NaCl, 5% Glycerol and 0.001% Tween.
533 Approximately 4-6 μL of each sample was loaded in a fused silica capillary
534 (NanoTemper Technologies). Measurements were performed at room temperature in a
535 Monolith NT.115 instrument at a constant LED power of 65% and MST power of 60%.
536 Measurements were performed repeatedly on independent protein preparations to
537 ensure reproducibility. The data were analysed by plotting peptide concentrations
538 against percent changes of normalized fluorescence. Curve fitting was performed using
539 PALMIST software (Scheuermann et al., 2016).
540

541 **Bacterial strains and culture**

542 A list of bacterial strains used in this study are provided in Table S1. *Escherichia coli*
543 DH5α, which was used for general cloning, was cultured in lysogeny broth (LB) with the
544 appropriate antibiotics at 37°C (shaking at 230 rpm for liquid cultures). *Xoo* strains were
545 routinely cultured at 28°C on peptone sucrose agar (PSA) with the appropriate
546 antibiotics unless otherwise indicated. Nutrient broth or agar was initially used to
547 generate the mutant strains. When needed, sucrose was added to a final concentration
548 of 5% and antibiotics were added. For proteomic analysis, cells were grown on XOM2

549 (Tsuge et al., 2002) agar, a plant-mimicking medium. Cephalexin was used at 20
550 μg/mL, kanamycin at 50 μg/mL, and geneticin at 50 μg/mL.
551
552 **Protein extraction**
553 *Xoo* proteins were prepared from strains grown on XOM2 agar plates, which was found
554 to induce *raxX* expression. After incubation at 28°C for 2 days, the fully-grown cells
555 were scraped from the plates and re-suspended in 30 mL of water to loosen the
556 extracellular polysaccharide matrix containing the secretome. The cells were pelleted by
557 centrifugation (12k rpm, 45 min, 4°C). The supernatants, which contained the secreted
558 proteins, were harvested and concentrated to 0.5-1 mL using Amicon® Ultra Centrifugal
559 Filters Ultracel®-3K (Millipore, Burlington, MA, cat#UFC900324). Total protein was also
560 extracted from the cell pellet. The cells were resuspended and lysed by sonication in
561 lysis buffer (25mM Tris pH 8, 300mM NaCl, 1mM PMSF, 2.5 mM EDTA, and 1mg/ml
562 lysozyme). Soluble proteins were separated by centrifugation (12k rpm, 45 min, 4°C).
563 All of the samples for mass spectrometry were digested with 1 μg of trypsin
564 (Promega, Madison, WI) in the presence of 5 mM DTT. The tryptic peptides were
565 desalted with a C18 column (Harvard apparatus, Holliston, MA, cat#74-4601) and
566 eluted with 80 % acetonitrile, 0.1 % formic acid.
567
568 **LC-SRM-MS Analysis**
569 The SRM targeted proteomic assays were performed, as described previously (Batth et
570 al., 2014), on an Agilent 6460 QQQ mass spectrometer system coupled with an Agilent
571 1290 UHPLC system (Agilent Technologies, Santa Clara, CA). Peptides were separated

572 on an Ascentis Express Peptide C18 column [2.7-mm particle size, 160-Å pore size, 5-
573 cm length × 2.1-mm inside diameter (ID), coupled to a 5-mm × 2.1-mm ID guard column
574 with same particle and pore size, operating at 60°C; Sigma-Aldrich, St. Louis, MO]
575 operated at a flow rate of 0.4 ml/min via the following gradient: initial conditions were
576 95% solvent A (0.1% formic acid), 5% solvent B (99.9% acetonitrile, 0.1% formic acid).
577 Solvent B was increased to 35% over 5 min, and was then increased to 80% over 0.2
578 min, and held for 2 min at a flow rate of 0.6 mL/min, followed by a ramp back down to
579 5% B over 0.5 min where it was held for 1.5 min to re-equilibrate the column to original
580 conditions. The eluted peptides were ionized via an Agilent Jet Stream ESI source
581 operating in positive ion mode with the following source parameters: gas temperature =
582 250°C, gas flow = 13 liters/min, nebulizer pressure = 35 psi, sheath gas temperature =
583 250°C, sheath gas flow = 11 liters/min, capillary voltage = 3500 V, nozzle voltage = 0 V.
584 The data were acquired using Agilent MassHunter version B.08.02. Acquired SRM data
585 were processed by using Skyline software version 3.70 (MacCoss Lab Software,
586 Seattle, WA).
587
588 **Immunoblotting**
589 The proteins were separated by SDS-PAGE, transferred to PVDF membranes (Bio Rad,
590 Hercules, CA cat#162-0177) by electrophoresis and then analyzed by immunoblot using
591 standard procedures. RaxX was detected using an anti-RaxX antibody that was raised
592 in rabbit against RaxX11 (PPGANPKHDPP), derived from residues 43-53 of the 60-
593 residue RaxX precursor (GenScript, Piscataway, NJ). Alkaline phosphatase conjugated
594 anti-rabbit IgG (Sigma, cat#A3687) was used as secondary antibody and CDP-*Star*

595 (Roche, Basel, Switzerland, cat#12041677001) was used as substrate. The anti-RaxX
596 and anti-rabbit IgG antibodies were used at dilutions of 1:2000 and 1:20,000,
597 respectively. The membranes were exposed to X-ray films or visualized using the Gel-
598 Doc XR$^+$ system (Bio-Rad).
599
600 **Identification of the *pct* locus**
601 PctB (PXO_RS14825) was identified by NCBI Protein BLAST analysis of the PXO99
602 genome (NC_010717.2) using the RaxB (PXO_RS06015) N-terminal 150 residues as
603 query under the default settings. PctP (PXO_RS14830) and PctA (PXO_RS14840)
604 were identified by algorithms from NCBI in the rhomboid family (CDD:304416) and the
605 type_I_hylD (CDD:330454) domain classification, respectively. Pct-92 (PXO_RS14845)
606 and Pct-75 (PXO_RS14850) were annotated as hypothetical proteins.
607
608 ***Xoo* mutation and complementation**
609 *Xoo* mutants were generated in the Philippine race 6 strain PXO99^A (referred to as
610 PXO99 in this manuscript; Hopkins et al., 1992). The mutant strain Δ*raxX* and the
611 complemented strain Δ*raxX*(p*raxX*) used in this study were previously reported (Pruitt et
612 al., 2015). The rest of the mutant strains: Δ*raxB*, Δ*pctB*, Δ*raxB* Δ*pctB*, Δ*raxA*, Δ*pctA*,
613 and Δ*raxA* Δ*pctA,* were generated by double homologous recombination using the
614 pUFR80 suicide vector (Castañeda et al., 2005). Briefly, two flanking sequences
615 upstream and downstream of the target gene were independently PCR-amplified with
616 their respective primer sets A, B and C, D (Table S2) using Phusion High-Fidelity DNA
617 polymerase (Thermo Scientific, Waltham, MA). Both PCR products were fused together

618 by overlap extension PCR (Horton et al., 1989) using external primers A and D. This
619 PCR product was then cloned into pUFR80 using the sites EcoRI/HindIII or
620 BamHI/HindIII. The resultant plasmids, which were verified by sequencing, were
621 electroporated into PXO99 (Δ*raxB* or Δ*raxA* was used instead for generation of the
622 Δ*raxB* Δ*pctB* or Δ*raxA* Δ*pctA* double mutant, respectively). The electroporated cells
623 were then plated onto nutrient agar (NA) with kanamycin (50 μg/mL) and grown at 28°C
624 for 5-6 days. Positive integrants were screened by PCR, grown in nutrient broth without
625 kanamycin overnight, and then plated onto NA containing 5% sucrose to select for the
626 second crossover event. Colonies were analyzed by PCR to identify deletion mutants
627 and verified by sequencing the PCR product.
628 For complementation, all of the plasmids (listed in Table S3) were constructed
629 using standard recombinant DNA techniques using the primers listed in Table S2.
630 p*raxX-ha* was generated by cloning the *raxX* coding sequence into pENTR/D-TOPO
631 (Invitrogen, Carlsbad, CA), which was then recombined into pLN615, a gateway
632 destination vector containing an HA tag (Guo et al., 2009). p*raxSTAB* and p*pctPB* were
633 derived from pVSP61 (Loper and Lindow, 1994), into which the indicated gene clusters
634 and 0.4 kb of the upstream sequence, presumed to contain the native promoter, were
635 cloned. Expression of *raxSTAB* and *pctPB* were chosen instead of independent
636 expression of *raxB* and *pctB*, respectively, to account for potential translational coupling
637 with *raxA* and *pctP*, respectively. Site-directed mutagenesis of catalytic residues of the
638 RaxB peptidase domain and residues of the RaxX leader were generated in p*raxSTAB*
639 and p*raxX*, respectively. All of the plasmids were verified by sequencing. The plasmids
640 were transformed into *Xoo* competent cells by electroporation, plated onto PSA with the

appropriate antibiotic, and grown at 28°C. Colonies were analyzed by PCR and verified by sequencing the PCR product.

Rice plants

The *Oryza sativa* ssp. *japonica* rice variety TP309 and a transgenic TP309 line derived from I106-17 (XA21-TP309), which carries the *Xa21* gene driven by its own promoter (Song et al., 1995) were used for rice inoculations. Native TP309 does not contain *Xa21*. TP309 and XA21-TP309 rice plants were grown as previously described (Pruitt et al., 2015). Briefly, seeds were germinated in distilled water at 28°C for 1 week then transplanted to sandy soil in 5.5-inch square pots (3 seedlings per pot). Plants were grown in tubs filled with fertilizer water in a greenhouse. Six-week old plants were then transferred to a growth chamber at least 2 days prior to inoculation. The growth chamber was set to 28°C/24°C, 80%/85% humidity, and 14/10-hour lighting for the day/night cycle.

Rice inoculation

Xoo strains were cultured on PSA plates with appropriate antibiotics at 28°C. Bacteria from the plates were resuspended in sterile water at a density of 10^8 colony-forming units (CFU)/mL and then inoculated onto rice plants using the scissor clipping method (Kauffman, 1973). Briefly, surgical scissors were dipped in bacterial suspension and used to clip the tips of the two uppermost expanded leaves in each tiller, representing one biological replicate. The length (cm) of the water-soaked lesions extending from the site of inoculation were measured 14 days after inoculation. The lesions of at least 8

biological replicates, each a mean of the lesions formed on the two leaves, were measured. At least 3 independent experiments were performed with similar results unless indicated otherwise.

Analysis of bacterial growth *in planta* was performed as previously described (Bahar et al., 2014) with minor modifications. Briefly, leaves (10-cm section from the site of inoculation) were harvested for each sample set at each time point. The two leaf sections from each tiller, representing one biological replicate, were cut to 2 mm pieces and incubated in sterile water for 2 hours at 28°C shaking at 230 rpm. This suspension was serially diluted, plated onto PSA plates with cephalexin (20 μg/mL), and incubated at 28°C. Colonies were counted 2 days later and the cell number per 10-cm leaf section was calculated. Three to four biological replicates, each a mean number of colonies from 4 technical replicates, were measured for each data point. Three independent experiments were performed with similar results.

For *in planta* bacterial gene expression analysis, TP309 leaves were harvested 6 days after inoculation. The leaves were cut 4 cm from the site of inoculation and the 4-cm section from two leaves of each tiller, representing one biological replicate, were snap-frozen in liquid nitrogen and processed as described below.

RNA Extraction and RT-qPCR

Total RNA was extracted from homogenized rice leaf tissue using TRIzol reagent (Invitrogen) following the manufacturer's instructions and then treated with the TURBO DNA-free kit (Ambion) to remove residual genomic DNA. cDNA was synthesized using the High-Capacity cDNA Reverse Transcription Kit (Applied Biosystems, Foster City,

CA) according to the manufacturer's instructions. Quantitative PCR (qPCR) was performed on a Bio-Rad CFX96 Real-Time System coupled to a C1000 Thermal Cycler (Bio-Rad) using the iTaq Universal SYBR Green Supermix (Bio-Rad) and 100 ng of cDNA. The primers used are listed in Table S2. The 2^(-ΔΔCt) method was used to calculate the relative changes in gene expression normalized to the *ampC2* reference gene control and the PXO99 wildtype strain. Three biological replicates, each a mean of two technical replicates, were analyzed. Three independent experiments were performed with similar results.

Sequence analysis and visualization

The C- and H-motifs of the RaxB and PctB peptidase domains were identified from alignments of the peptidase domain of the *E. coli* colicin V transporter CvaB (CAA40744.1; Wu and Tai, 2004), the *Leuconostoc mesenteroides* mesentericin B105 and Y105 transporter MesD (CAA57402.1; Aucher et al., 2005; Morisset and Frère, 2002), the *Streptococcus pneumoniae* competence-stimulating peptide transporter ComA (AAA69510.1; Ishii et al., 2006), the *Lactococcus lactis* lactococcin G transporter LagD (ACR43772.1; Håvarstein et al., 1995), the *Lactococcus lactis* lacticin 481 transporter LctT (AAC72259.1; Furgerson Ihnken et al., 2008), and the *Staphylococcus warneri* nukacin ISK-1 transporter NukT (NP_940774.2; Nishie et al., 2009), as well as the peptidase-like domain of the *Aggregatibacter actinomycetemcomitans* leukotoxin transporter LktB (CAA37906.1; Guthmiller et al., 1995), and the *E. coli* alpha-hemolysin transporter HlyB (KKA61973.1; Lecher et al., 2012). The alignment was performed

using the default settings in Clustal Omega (European Bioinformatics Institute; EMBL-EBI; Sievers et al., 2011).

The sequence logo of the RaxX leader was constructed using WebLogo (Crooks et al., 2004) with the predicted leader sequence of RaxX alleles from various *Xanthomonas* species identified by Pruitt et al. (2017). The RaxX leader was aligned with the predicted leader of the candidate PctB substrates Pct-92 and Pct-75 as well as the experimentally verified leader sequences from the *E. coli* colicin V precursor CvaC (AAX22078.1; Håvarstein et al., 1994), the *Leuconostoc mesenteroides* mesentericin B105 and Y105 precursors MesB and MesY (AAD54223.1 and AAP37395.1, respectively; Morisset and Frère, 2002; Aucher et al., 2005); the *Streptococcus pneumoniae* competence-stimulating peptide precursor ComC (AAC44895.1; Ishii et al., 2006), the *Lactococcus lactis* lactococcin alpha and beta precursors LagA and LagB, respectively (ACR43769.1 and ACR43770.1, respectively; Håvarstein et al., 1995), the *Lactococcus lactis* lacticin 481 precursor LctA (AAC72257.1; Furgerson Ihnken et al., 2008), and the *Staphylococcus warneri* nukacin ISK-1 precursor NukA (NP_940772.1; Nishie et al., 2009).

Statistical analysis

Statistical analysis was performed using JMP Pro 13 (SAS Institute Inc., Cary, NC) or GraphPad Prism 7 (GraphPad Software, La Jolla, CA) and specified in figure legends. Differences were considered to be significant when $p < 0.05$.

ACKNOWLEDGMENTS

This work was supported by NIH GM59962, NIH GM122968, and NSF PGRP grant IOS-1237975. This work was also partially supported by the Office of Biological and Environmental Research's Genomic 275 Science program within the U.S. Department of Energy Office of Science, under award number DE-AC02-05CH11231.

AUTHOR CONTRIBUTIONS

D.D.L., A.J., O.B., C.P., Y.B., and P.C.R. conceived and designed the research. D.D.L., A.J., Y.C., K.P., R.P., L.C., K.L., and C.A. performed experiments. D.D.L., A.J., Y.C., K.P., and V.S. analyzed data. D.D.L., A.J., V.S., and P.C.R. wrote the manuscript with assistance and feedback from the other authors.

DECLARATION OF INTERESTS

The authors declare no competing interests.

REFERENCES

Amano, Y., Tsubouchi, H., Shinohara, H., Ogawa, M., and Matsubayashi, Y. (2007). Tyrosine-sulfated glycopeptide involved in cellular proliferation and expansion in Arabidopsis. Proc. Natl. Acad. Sci. *104*, 18333–18338.

754 Arnison, P.G., Bibb, M.J., Bierbaum, G., Bowers, A.A., Bugni, T.S., Bulaj, G., Camarero,
755 J.A., Campopiano, D.J., Challis, G.L., Clardy, J., et al. (2013). Ribosomally
756 synthesized and post-translationally modified peptide natural products: overview and
757 recommendations for a universal nomenclature. Nat. Prod. Rep. *30*, 108–160.
758 Aucher, W., Lacombe, C., Héquet, A., Frère, J., and Berjeaud, J.M. (2005). Influence of
759 amino acid substitutions in the leader peptide on maturation and secretion of
760 mesentericin Y105 by Leuconostoc mesenteroides. J. Bacteriol. *187*, 2218–2223.
761 Bahar, O., Pruitt, R., Luu, D.D., Schwessinger, B., Daudi, A., Liu, F., Ruan, R.,
762 Fontaine-Bodin, L., Koebnik, R., and Ronald, P. (2014). The Xanthomonas Ax21
763 protein is processed by the general secretory system and is secreted in association
764 with outer membrane vesicles. PeerJ *2*, e242.
765 Batth, T.S., Singh, P., Ramakrishnan, V.R., Sousa, M.M.L., Chan, L.J.G., Tran, H.M.,
766 Luning, E.G., Pan, E.H.Y., Vuu, K.M., Keasling, J.D., et al. (2014). A targeted
767 proteomics toolkit for high-throughput absolute quantification of Escherichia coli
768 proteins. Metab. Eng. *26*, 48–56.
769 Burkhart, B.J., Kakkar, N., Hudson, G.A., van der Donk, W.A., and Mitchell, D.A. (2017).
770 Chimeric leader peptides for the generation of non-natural hybrid RiPP products.
771 ACS Cent. Sci. *3*, 629–638.
772 Caetano, T., Barbosa, J., Möesker, E., Süssmuth, R.D., and Mendo, S. (2014).
773 Bioengineering of lanthipeptides in Escherichia coli: assessing the specificity of
774 lichenicidin and haloduracin biosynthetic machinery. Res. Microbiol. *165*, 600–604.
775 Castañeda, A., Reddy, J.D., El-Yacoubi, B., and Gabriel, D.W. (2005). Mutagenesis of
776 all eight *avr* Genes in Xanthomonas campestris pv. campestris had no detected

effect on pathogenicity, but one *avr* gene affected race specificity. Mol. Plant. Microbe Interact. *18*, 1306–1317.

Crooks, G.E., Hon, G., Chandonia, J.M., and Brenner, S.E. (2004). WebLogo: a sequence logo generator. Genome Res *14*, 1188–1190.

da Silva, F.G., Shen, Y., Dardick, C., Burdman, S., Yadav, R.C., de Leon, A.L., and Ronald, P.C. (2004). Bacterial genes involved in type I secretion and sulfation are required to elicit the rice Xa21-mediated innate immune response. Mol. Plant. Microbe Interact. *17*, 593–601.

Dardick, C., Schwessinger, B., and Ronald, P. (2012). Non-arginine-aspartate (non-RD) kinases are associated with innate immune receptors that recognize conserved microbial signatures. Curr. Opin. Plant Biol. *15*, 358–366.

Dirix, G., Monsieurs, P., Dombrecht, B., Daniels, R., Marchal, K., Vanderleyden, J., and Michiels, J. (2004). Peptide signal molecules and bacteriocins in Gram-negative bacteria: a genome-wide in silico screening for peptides containing a double-glycine leader sequence and their cognate transporters. Peptides *25*, 1425–1440.

Doblas, V.G., Smakowska-Luzan, E., Fujita, S., Alassimone, J., Barberon, M., Madalinski, M., Belkhadir, Y., and Geldner, N. (2017). Root diffusion barrier control by a vasculature-derived peptide binding to the SGN3 receptor. Science *355*, 280–284.

Farzan, M., Mirzabekov, T., Kolchinsky, P., Wyatt, R., Cayabyab, M., Gerard, N.P., Gerard, C., Sodroski, J., and Choe, H. (1999). Tyrosine sulfation of the amino terminus of CCR5 facilitates HIV-1 entry. Cell *96*, 667–676.

799 Freeman, M. (2014). The rhomboid-like superfamily: molecular mechanisms and
800 biological roles. Annu. Rev. Cell Dev. Biol. *30*, 235–254.
801 Furgerson Ihnken, L.A., Chatterjee, C., and van der Donk, W.A. (2008). In vitro
802 reconstitution and substrate specificity of a lantibiotic protease. Biochemistry *47*,
803 7352–7363.
804 Guo, M., Tian, F., Wamboldt, Y., and Alfano, J.R. (2009). The majority of the type III
805 effector inventory of Pseudomonas syringae pv. tomato DC3000 can suppress plant
806 immunity. Mol. Plant-Microbe Interact. *22*, 1069–1080.
807 Guthmiller, J.M., Kolodrubetz, D., and Kraig, E. (1995). Mutational analysis of the
808 putative leukotoxin transport genes in actinobacillus actinomycetemcomitans.
809 Microb. Pathog. *18*, 307–321.
810 Han, S.-W., Lee, S.-W., Bahar, O., Schwessinger, B., Robinson, M.R., Shaw, J.B.,
811 Madsen, J.A., Brodbelt, J.S., and Ronald, P.C. (2012). Tyrosine sulfation in a Gram-
812 negative bacterium. Nat. Commun. *3*, 1153.
813 Håvarstein, L.S., Holo, H., and Nes, I.F. (1994). The leader peptide of colicin V shares
814 consensus sequences with leader peptides that are common among peptide
815 bacteriocins produced by Gram-positive bacteria. Microbiology *140*, 2383–2389.
816 Håvarstein, L.S., Diep, D.B., and Nes, I.F. (1995). A family of bacteriocin ABC
817 transporters carry out proteolytic processing of their substrates concomitant with
818 export. Mol. Microbiol. *16*, 229–240.
819 Hopkins, C.M., White, F.F., Choi, S.H., Guo, A., and Leach, J.E. (1992). Identification of
820 a family of avirulence genes from Xanthomonas oryzae pv. oryzae. Mol. Plant
821 Microbe Interact. *5*, 451-459.

822 Horton, R.M., Hunt, H.D., Ho, S.N., Pullen, J.K., and Pease, L.R. (1989). Engineering
823 hybrid genes without the use of restriction enzymes: gene splicing by overlap
824 extension. Gene *77*, 61–68.
825 Ishii, S., Yano, T., and Hayashi, H. (2006). Expression and characterization of the
826 peptidase domain of Streptococcus pneumoniae ComA, a bifunctional ATP-binding
827 cassette transporter involved in quorum sensing pathway. J. Biol. Chem. *281*, 4726–
828 4731.
829 Ishii, S., Yano, T., Ebihara, A., Okamoto, A., Manzoku, M., and Hayashi, H. (2010).
830 Crystal structure of the peptidase domain of Streptococcus ComA, a bifunctional
831 ATP-binding cassette transporter involved in the quorum-sensing pathway. J. Biol.
832 Chem. *285*, 10777–10785.
833 Kanonenberg, K., Schwarz, C.K.W., and Schmitt, L. (2013). Type I secretion systems -
834 a story of appendices. Res. Microbiol. *164*, 596–604.
835 Kauffman, H.E., Reddy, A.P.K., Hsieh, S.P.Y., and Merca, S.D. (1973). An improved
836 technique for evaluating resistance of rice varieties to Xanthomonas oryzae. Plant
837 Dis. Reptr. *57*, 537-541.
838 Kotake, Y., Ishii, S., Yano, T., Katsuoka, Y., and Hayashi, H. (2008). Substrate
839 recognition mechanism of the peptidase domain of the quorum-sensing-signal-
840 producing ABC transporter ComA from Streptococcus. Biochemistry *47*, 2531–2538.
841 Lawton, E.M., Cotter, P.D., Hill, C., and Ross, R.P. (2007). Identification of a novel two-
842 peptide lantibiotic, haloduracin, produced by the alkaliphile Bacillus halodurans C-
843 125. FEMS Microbiol. Lett. *267*, 64–71.

844 Lecher, J., Schwarz, C.K.W., Stoldt, M., Smits, S.H.J., Willbold, D., and Schmitt, L.
845 (2012). An RTX transporter tethers its unfolded substrate during secretion via a
846 unique N-terminal domain. Structure *20*, 1778–1787.
847 Levengood, M.R., Patton, G.C., and van der Donk, W.A. (2007). The leader peptide is
848 not required for post-translational modification by lacticin 481 synthetase. J. Am.
849 Chem. Soc. *129*, 10314–10315.
850 Loper, J.E., and Lindow, S.E. (1994). A biological sensor for iron available to bacteria in
851 their habitats on plant surfaces. Appl. Environ. Microbiol. *60*, 1934–1941.
852 Matsubayashi, Y., and Sakagami, Y. (1996). Phytosulfokine, sulfated peptides that
853 induce the proliferation of single mesophyll cells of Asparagus officinalis L. Proc.
854 Natl. Acad. Sci. *93*, 7623–7627.
855 Matsuzaki, Y., Ogawa-Ohnishi, M., Mori, A., and Matsubayashi, Y. (2010). Secreted
856 peptide signals required for maintenance of root stem cell niche in Arabidopsis.
857 Science *329*, 1065–1067.
858 Ménard, R., Carrière, J., Laflamme, P., Plouffe, C., Khouri, H.E., Vernet, T., Tessier,
859 D.C., Thomas, D.Y., Storer, A.C. (1991). Contribution of the glutamine 19 side chain
860 to transition-state stabilization in the oxyanion hole of papain. Biochemistry *30*,
861 8924–8928.
862 Morisset, D., and Frère, J. (2002). Heterologous expression of bacteriocins using the
863 mesentericin Y105 dedicated transport system by Leuconostoc mesenteroides.
864 Biochimie *84*, 569–576.

865 Nakayama, T., Shinohara, H., Tanaka, M., Baba, K., Ogawa-Ohnishi, M., and
866 Matsubayashi, Y. (2017). A peptide hormone required for Casparian strip diffusion
867 barrier formation in Arabidopsis roots. Science *355*, 284–286.
868 Nishie, M., Shioya, K., Nagao, J., Jikuya, H., and Sonomoto, K. (2009). ATP-dependent
869 leader peptide cleavage by NukT, a bifunctional ABC transporter, during lantibiotic
870 biosynthesis. J. Biosci. Bioeng. *108*, 460–464.
871 Oman, T.J., and van der Donk, W.A. (2010). Follow the leader: the use of leader
872 peptides to guide natural product biosynthesis. Nat. Chem. Biol. *6*, 9–18.
873 Oman, T.J., Knerr, P.J., Bindman, N.A., Velásquez, J.E., and van der Donk, W.A.
874 (2012). An engineered lantibiotic synthetase that does not require a leader peptide
875 on its substrate. J. Am. Chem. Soc. *134*, 6952–6955.
876 Pruitt, R.N., Schwessinger, B., Joe, A., Thomas, N., Liu, F., Albert, M., Robinson, M.R.,
877 Chan, L.J.G., Luu, D.D., Chen, H., et al. (2015). The rice immune receptor XA21
878 recognizes a tyrosine-sulfated protein from a Gram-negative bacterium. Sci. Adv. *1*,
879 e1500245.
880 Pruitt, R.N., Joe, A., Zhang, W., Feng, W., Stewart, V., Schwessinger, B., Dinneny, J.R.,
881 and Ronald, P.C. (2017). A microbially derived tyrosine-sulfated peptide mimics a
882 plant peptide hormone. New Phytol. *215*, 725–736.
883 Scheuermann, T.H., Padrick, S.B., Gardner, K.H., and Brautigam, C.A. (2016). On the
884 acquisition and analysis of microscale thermophoresis data. Anal. Biochem. *496*,
885 79–93.

886 Scholz, J., Besir, H., Strasser, C., and Suppmann, S. (2013). A new method to
887 customize protein expression vectors for fast, efficient and background free parallel
888 cloning. BMC Biotechnol. *13*, 1–11.
889 Schwessinger, B., Li, X., Ellinghaus, T.L., Chan, L.J.G., Wei, T., Joe, A., Thomas, N.,
890 Pruitt, R., Adams, P.D., Chern, M.S., et al. (2016). A second-generation expression
891 system for tyrosine-sulfated proteins and its application in crop protection. Integr.
892 Biol. *8*, 542–545.
893 Sievers, F., Wilm, A., Dineen, D., Gibson, T.J., Karplus, K., Li, W., Lopez, R.,
894 McWilliam, H., Remmert, M., Söding, J., et al. (2011). Fast, scalable generation of
895 high-quality protein multiple sequence alignments using Clustal Omega. Mol. Syst.
896 Biol. *7*, 539. doi:10.1038/msb.2011.75.
897 Song, W.Y., Wang, G.L., Chen, L.L., Kim, H.S., Pi, L.Y., Holsten, T., Gardner, J., Wang,
898 B., Zhai, W.X., Zhu, L.H., et al. (1995). A receptor kinase-like protein encoded by the
899 rice disease resistance gene, Xa21. Science *270*, 1804–1806.
900 Stone, M.J., Chuang, S., Hou, X., Shoham, M., and Zhu, J.Z. (2009). Tyrosine sulfation:
901 an increasingly recognised post-translational modification of secreted proteins. New
902 Biotechnol. *25*, 299–317.
903 Tsuge, S., Furutani, A., Fukunaka, R., Oku, T., Tsuno, K., Ochiai, H., Inoue, Y., Kaku,
904 H., and Kubo, Y. (2002). Expression of Xanthomonas oryzae pv. oryzae hrp genes
905 in XOM2, a novel synthetic medium. J. Gen. Plant Pathol. *68*, 363–371.
906 Wang, J., Li, H., Han, Z., Zhang, H., Wang, T., Lin, G., Chang, J., Yang, W., and Chai,
907 J. (2015). Allosteric receptor activation by the plant peptide hormone phytosulfokine.
908 Nature *525*, 265–268.

909 Wei, T., Chern, M., Liu, F., and Ronald, P.C. (2016). Suppression of bacterial infection
910 in rice by treatment with a sulfated peptide. Mol. Plant Pathol. *17*, 1493–1498.
911 Wienken, C.J., Baaske, P., Rothbauer, U., Braun, D., and Duhr, S. (2010). Protein-
912 binding assays in biological liquids using microscale thermophoresis. Nat. Commun.
913 *1*, 1–7.
914 Wu, K.H., and Tai, P.C. (2004). Cys32 and His105 are the critical residues for the
915 calcium-dependent cysteine proteolytic activity of CvaB, an ATP-binding cassette
916 transporter. J. Biol. Chem. *279*, 901–909.
917 Wu, K.H., Hsieh, Y.H., and Tai, P.C. (2012). Mutational analysis of Cvab, an ABC
918 transporter involved in the secretion of active colicin V. PLoS ONE *7*, e35382.
919 doi:10.1371/journal.pone.0035382.
920 Xie, L., Miller, L.M., Chatterjee, C., Averin, O., Kelleher, N.L., van der Donk, W.A.
921 (2004). Lacticin 481: in vitro reconstitution of lantibiotic synthetase activity. Science
922 *303*, 679–682.
923 Zhang, L.H., Fath, M.J., Mahanty, H.K., Tai, P.C., and Kolter, R. (1995). Genetic
924 analysis of the colicin V secretion pathway. Genetics *141*, 25–32.
925

926 **FIGURE LEGENDS**

927

928 **Figure 1. Biosynthetic pathways of RiPPs and RaxX.**

929 (A) General RiPP biosynthetic pathway. The RiPP precursor and biosynthetic proteins
930 are ribosomally synthesized. The core, which becomes the final RiPP product, is post-
931 translationally modified by enzyme(s) encoded in the same genomic region. The N-

terminal leader is enzymatically removed by a protease and the modified core is exported by a transporter, releasing the mature bioactive RiPP.

(B) RaxX biosynthetic pathway. The RaxX precursor is ribosomally synthesized and the core is sulfated by the sulfotranferase RaxST encoded upstream. We hypothesize that the peptidase-containing ABC (ATP-binding cassette) transporter (PCAT) RaxB removes the N-terminal leader and transports the sulfated mature RaxX peptide through the type I secretion system (T1SS) composed of RaxB, the periplasmic adaptor protein RaxA, and the genetically unlinked outer membrane protein RaxC.

Figure 2. Sulfated RaxX peptide binds XA21ECD with high affinity.

Quantification of binding between sulfated (-sY, in red) and non-sulfated (-nY, in blue) RaxX21 and sulfated PSY1 (in grey) peptides with the XA21 ectodomain ($XA21^{ECD}$) by microscale thermophoresis (MST). Data points indicate the fraction of fluorescently labelled XA21 bound to the peptides during the assay (Fraction Bound [-]). The K_D and confidence intervals shown in brackets are indicated in nM. SE bars are representative of at least 2 independent measurements performed with independent protein preparations.

Figure 3. Mature RaxX is detected in *Xoo* supernatants.

(A) RaxX precursor sequence. Numbers above refer to the residue position relative to the predicted cleavage site; numbers below relative to the precursor peptide. Cleavage of RaxX after Gly-38, Gly-39 (in orange) would result in a leader with hydrophobic residues (in yellow) at conserved locations typical of PCAT substrates and a core

containing Tyr-41 (in green) sulfated by RaxST. Shown below this precursor are the synthetic RaxX peptide derivatives (RaxX21, RaxX16, RaxX13, and RaxX11) and the two tryptic peptide targets detected by selected reaction monitoring-mass spectrometry (SRM-MS).

(B-C) SRM-MS chromatograms of the non-processed precursor (B) and predicted mature (C) RaxX tryptic peptides detected from Δ*raxX*(p*raxX-His*) cell lysates or from PXO99 or Δ*raxX* supernatants. Lines correspond to individual SRM transitions monitored. Legend indicates the detected peptide y-series fragment ion.

(D) Quantification of the total peak area shown in C.

See also Figure S1.

Figure 4. Genetic map of candidate RaxX biosynthetic proteins.

(A) *raxX* is encoded upstream of the *raxSTAB* operon, containing genes for the RaxST sulfotransferase and components of a T1SS: the RaxA periplasmic adaptor protein and the RaxB PCAT.

(B) Genes for components of a second peptidase-containing transporter system are not genetically linked to *raxX*: *pctA* and *pctB*, encoding a periplasmic adaptor protein and PCAT, respectively.

Figure 5. The Δ*raxB* Δ*pctB* double mutant does not secrete RaxX, but secretion can be restored with the p*raxSTAB* plasmid.

(A-C) Rice plants were inoculated by scissor clipping with PXO99-derived strains.

977 (A) Bars represent the mean + SD of lesions (cm) measured 14 days post inoculation
978 (dpi) of TP309 (blue dots) or XA21-TP309 (red dots) plants (n = 21-28).
979 (B) Inoculated XA21-TP309 leaves 14 dpi. Scale bar, 1 cm.
980 (C) Bacterial densities in planta. Data points represent the mean log CFU per 10-cm
981 leaf section ± SE (n = 3).
982 (D) SRM-MS was used to detect the presence of mature RaxX in *Xoo* supernatants.
983 Bars represent the total peak area of the chromatograms shown in Figure S3C.
984 **p < 0.01; compared to PXO99 using Dunnett's test. Similar results were observed in 5
985 (A) or 2 (C) other experiments, except Δ*raxB* formed lesions comparable to PXO99 in
986 roughly half.
987 See also Figures S2 and S3.
988
989 **Figure 6. Mutation of the RaxB peptidase catalytic triad impairs RaxX maturation**
990 **and secretion.**
991 (A) Alignment of the peptidase C- and H-motifs of RaxB and PctB to select PCATs or
992 ABC transporters with a C39-like domain (CLD; listed in method details). Cys-His-
993 Asp/Asn catalytic triad highlighted in yellow, oxyanion hole Gln in green, and residues
994 common in at least 6 of the transporters in gray.
995 (B-D) Rice plants were inoculated by scissor clipping with the indicated strains.
996 (B) Bars represent the mean + SD of lesion measurements (cm) on TP309 (blue dots)
997 or XA21-TP309 (red dots) plants 14 dpi (n = 10-16).
998 (C) Inoculated XA21-TP309 leaves 14 dpi. Scale bar, 1 cm.

(D) Bacterial densities in planta. Data points represent the mean log CFU per 10-cm leaf section ± SE (n = 3). Performed at the same time as Figure 5C.

(E) SRM-MS chromatograms of mature RaxX tryptic peptide detected in supernatants from the Δ*raxB* Δ*pctB* double mutant-derived strains.

**p < 0.01; compared to PXO99 using Dunnett's test. Similar results were observed in 5 (B) or 2 (D) other independent experiments.

Figure 7. Mutation of the Gly-Gly cleavage site compromises RaxX maturation and secretion.

(A) Sequence logo of the leader from all *Xanthomonas* RaxX alleles. Conserved Gly-Gly preceding the cleavage site boxed in orange; hydrophobic residues in conserved positions typical of PCAT substrates boxed in black.

(B-C) Rice plants were inoculated by scissor clipping.

(B) Bars represent the mean + SD of lesion measurements (cm) on TP309 (blue dots) or XA21-TP309 (red dots) plants 14 dpi (n = 8-13). Similar results were observed in at least 6 independent experiments.

(C) Bars represent the mean log CFU/leaf section ± SE measured 14 dpi (n = 4).

(D) SRM-MS chromatograms of mature RaxX tryptic peptide detected in *Xoo* supernatants.

(E) Quantification of the total peak area shown in D.

*p < 0.05; **p < 0.01; compared to PXO99 using Dunnett's test.

See also Figure S4.

FIGURES

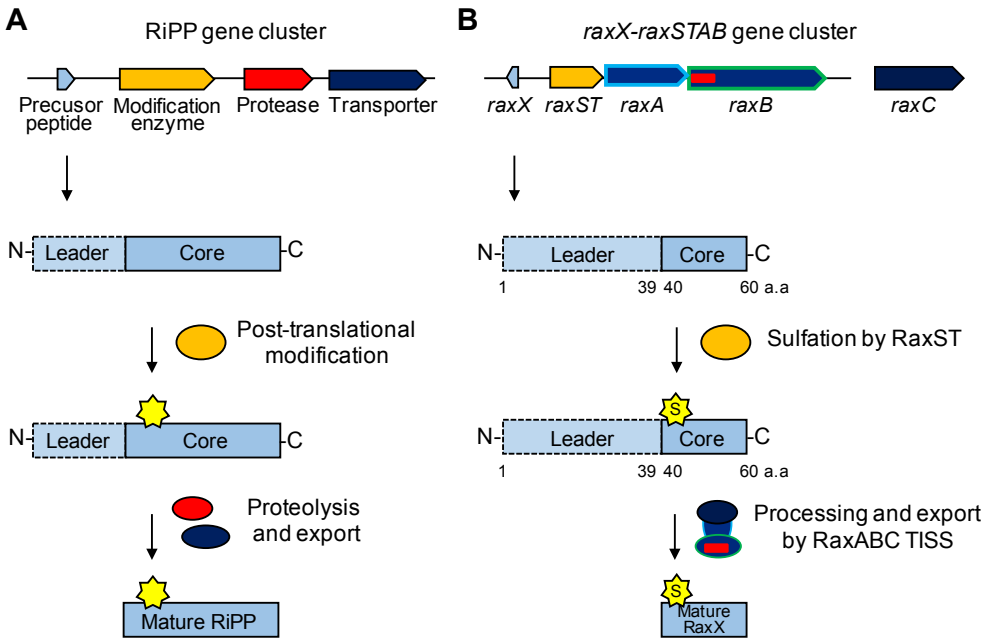

Figure 1

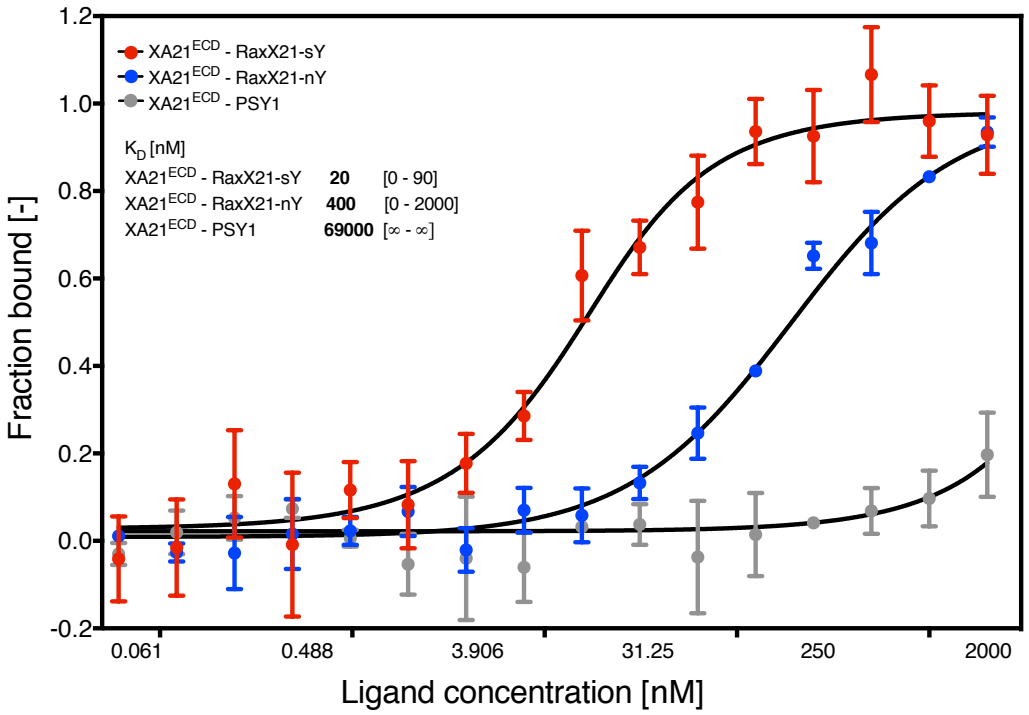
XA21ECD - RaxX21-sY
XA21ECD - RaxX21-nY
XA21ECD - PSY1
KD [nM]
XA21ECD - RaxX21-sY 20 [0 - 90]
XA21ECD - RaxX21-nY 400 [0 - 2000]
XA21ECD - PSY1 69000 [∞ - ∞]
Fraction bound [-]
1.2
1.0
0.8
0.6
0.4
0.2
0.0
-0.2
0.061
0.488
3.906
31.25
250
2000
Ligand concentration [nM]

Figure 2

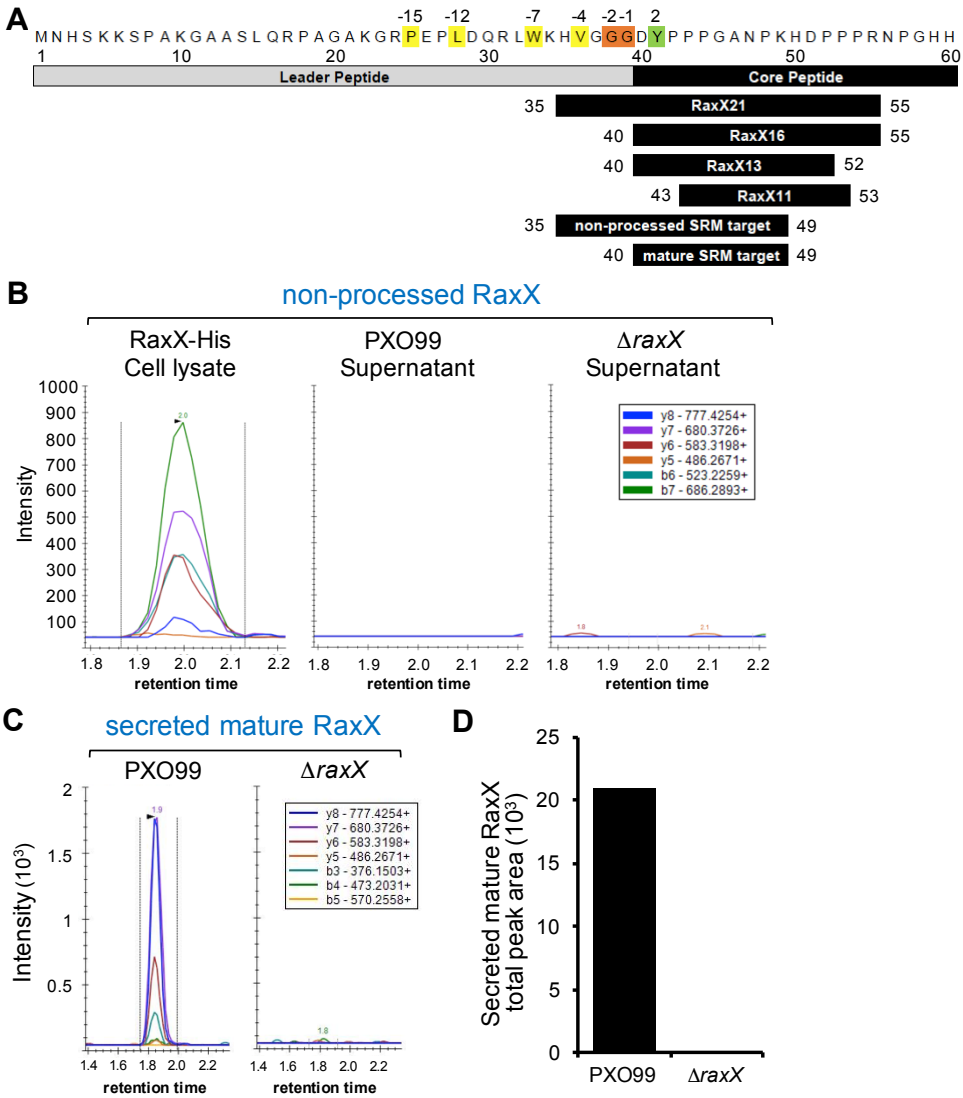
A
-15 -12 -7 -4 -2 -1 2
MNHSKKSPAKGAASLQRPAGAKGRPEPLDQRLWKHVGGGDYPPPGANPKHDPPPRNPGHH
1 10 20 30 40 50 60
Leader Peptide
Core Peptide
35 RaxX21 55
40 RaxX16 55
40 RaxX13 52
43 RaxX11 53
35 non-processed SRM target 49
40 mature SRM target 49
B
non-processed RaxX
RaxX-His Cell lysate
PXO99 Supernatant
ΔraxX Supernatant
Intensity
retention time
y8 - 777.4254+
y7 - 680.3726+
y6 - 583.3198+
y5 - 486.2671+
b6 - 523.2259+
b7 - 686.2893+
C
secreted mature RaxX
PXO99
ΔraxX
Intensity (10³)
y8 - 777.4254+
y7 - 680.3726+
y6 - 583.3198+
y5 - 486.2671+
b3 - 376.1503+
b4 - 473.2031+
b5 - 570.2558+
retention time
D
Secreted mature RaxX total peak area (10³)
PXO99
ΔraxX

Figure 3

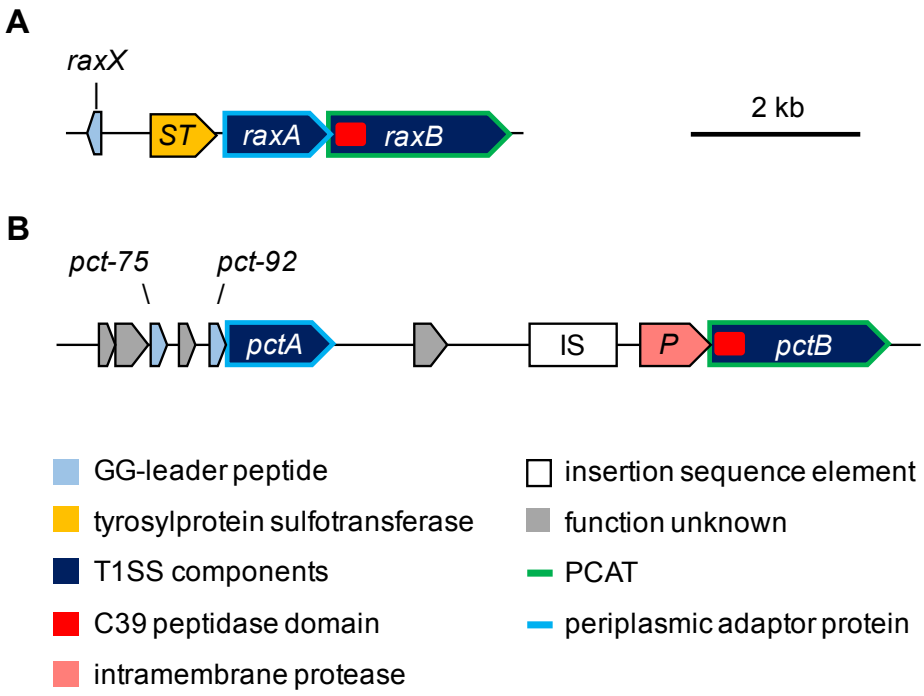
A
raxX
ST
raxA
raxB
2 kb
B
pct-75
pct-92
pctA
IS
P
pctB
GG-leader peptide
tyrosylprotein sulfotransferase
T1SS components
C39 peptidase domain
intramembrane protease
insertion sequence element
function unknown
PCAT
periplasmic adaptor protein

Figure 4

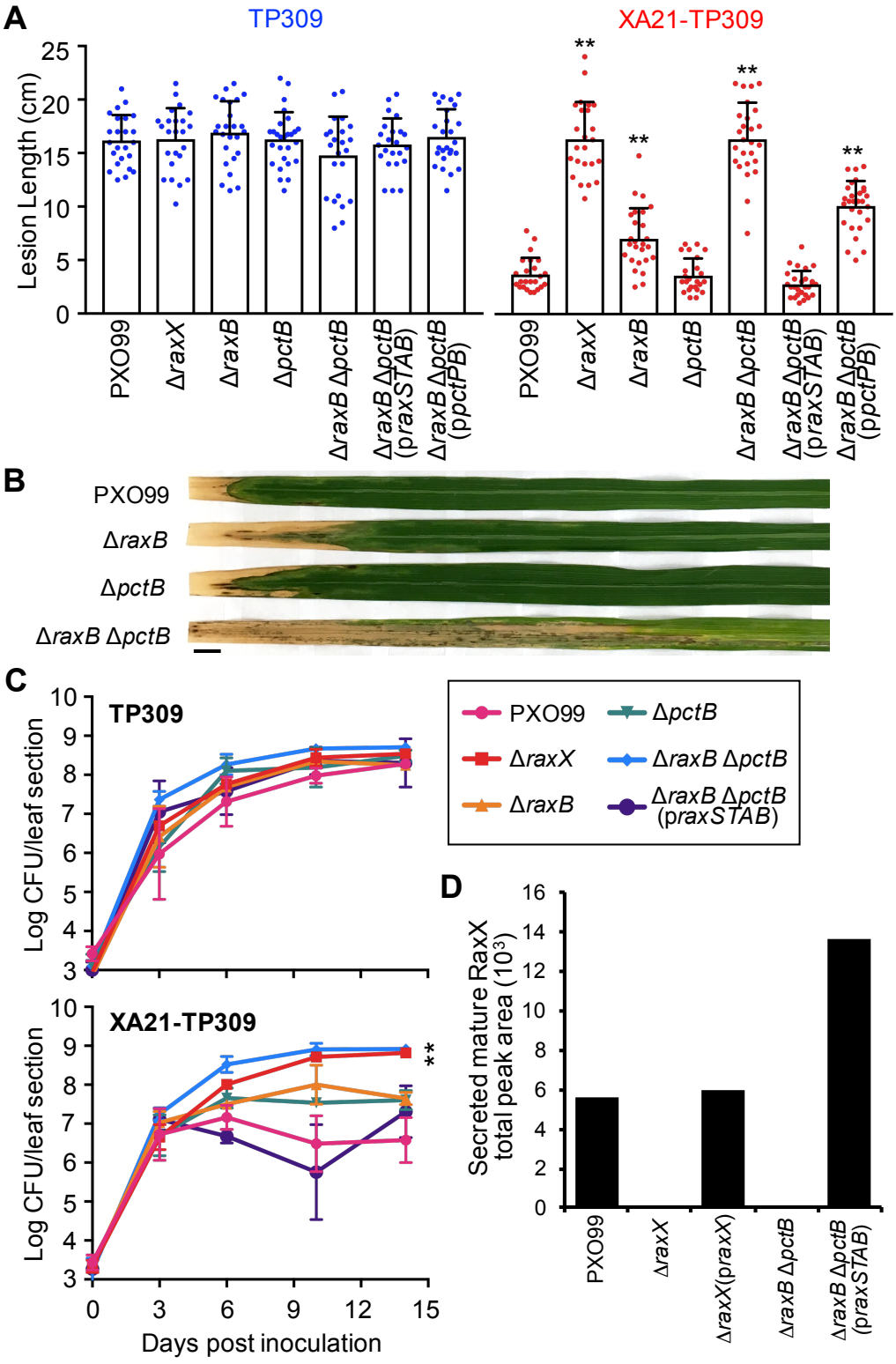
A
TP309
XA21-TP309
Lesion Length (cm)
PXO99
ΔraxX
ΔraxB
ΔpctB
ΔraxB ΔpctB
ΔraxB ΔpctB (praxSTAB)
ΔraxB ΔpctB (ppctPB)
B
PXO99
ΔraxB
ΔpctB
ΔraxB ΔpctB
C
TP309
XA21-TP309
Log CFU/leaf section
Days post inoculation
PXO99
ΔraxX
ΔraxB
ΔpctB
ΔraxB ΔpctB
ΔraxB ΔpctB (praxSTAB)
D
Secreted mature RaxX total peak area (10³)
PXO99
ΔraxX
ΔraxX(praxX)
ΔraxB ΔpctB
ΔraxB ΔpctB (praxSTAB)

Figure 5

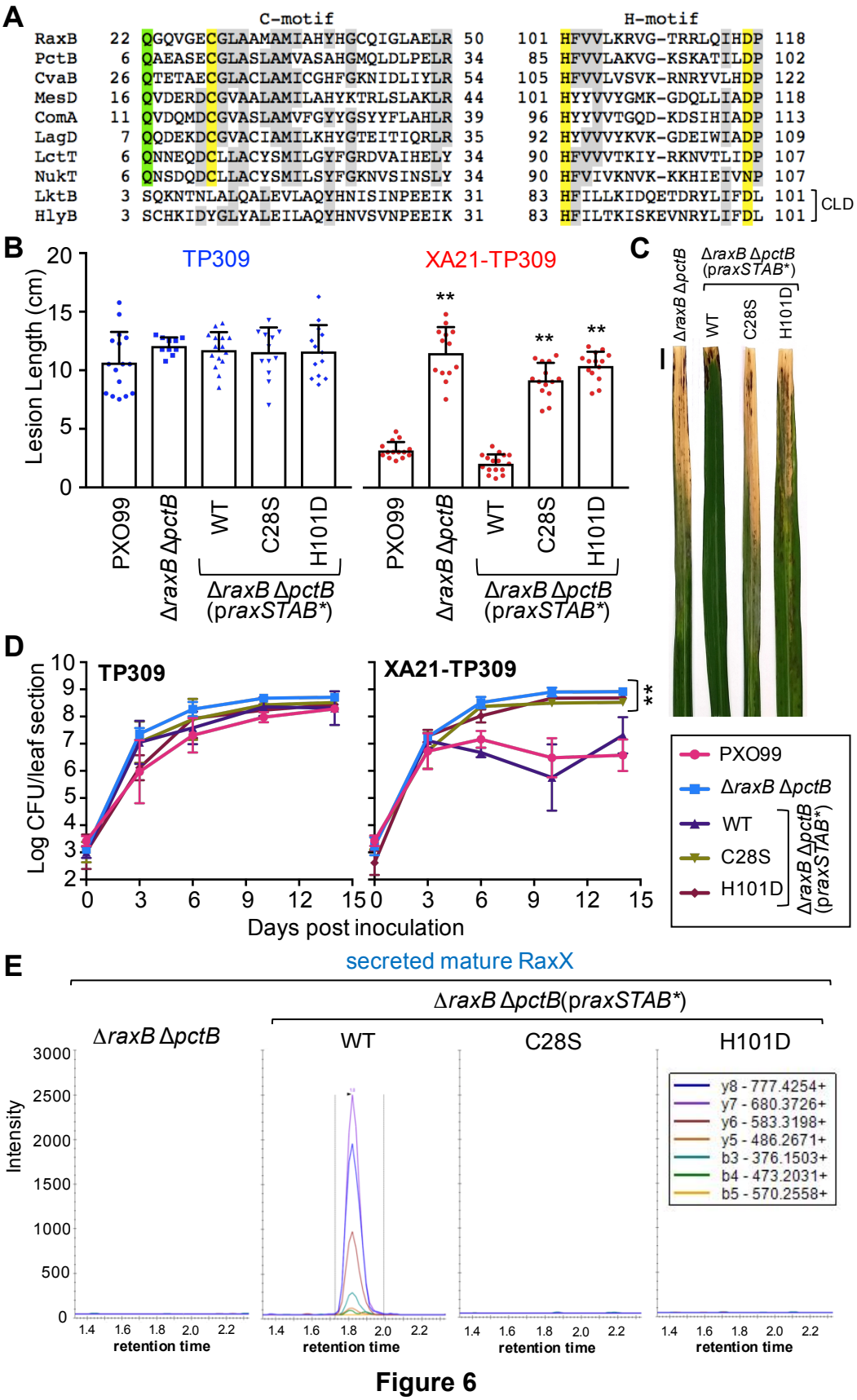
A
C-motif
H-motif
RaxB 22 QGQVGECGLAAMAMIAHYHGCQIGLAELR 50 101 HFVVLKRVG-TRRLQIHDP 118
PctB 6 QAEASECGLASLAMVASAHGMQLDLPELR 34 85 HFVVLAKVG-KSKATILDP 102
CvaB 26 QTETAECGLACLAMICGHFGKNIDLIYLR 54 105 HFVVLVSVK-RNRYVLHDP 122
MesD 16 QVDERDCGVAALAMILAHYKTRLSLAKLR 44 101 HYYVVYGMK-GDQLLIADP 118
ComA 11 QVDQMDCGVASLAMVFGYYGSYYFLAHLR 39 96 HYYVVTGQD-KDSIHIADP 113
LagD 7 QQDEKDCGVACIAMILKHYGTEITIQRLR 35 92 HYVVVYKVK-GDEIWIADP 109
LctT 6 QNNEQDCLLACYSMILGYFGRDVAIHELY 34 90 HFVVVTKIY-RKNVTLIDP 107
NukT 6 QNSDQDCLLACYSMILSYFGKNVSINSLY 34 90 HFVIVKNVK-KKHIEIVNP 107
LktB 3 SQKNTNLALQALEVLAQYHNISINPEEIK 31 83 HFILLKIDQETDRYLIFDL 101
HlyB 3 SCHKIDYGLYALEILAQYHNVSVNPEEIK 31 83 HFILTKISKEVNRYLIFDL 101
CLD
B
TP309
XA21-TP309
Lesion Length (cm)
PXO99
ΔraxB ΔpctB
WT
C28S
H101D
ΔraxB ΔpctB (praxSTAB*)
C
ΔraxB ΔpctB
ΔraxB ΔpctB (praxSTAB*)
D
TP309
XA21-TP309
Log CFU/leaf section
Days post inoculation
PXO99
ΔraxB ΔpctB
WT
C28S
H101D
E
secreted mature RaxX
ΔraxB ΔpctB(praxSTAB*)
ΔraxB ΔpctB
WT
C28S
H101D
Intensity
retention time
y8 - 777.4254+
y7 - 680.3726+
y6 - 583.3198+
y5 - 486.2671+
b3 - 376.1503+
b4 - 473.2031+
b5 - 570.2558+

Figure 6

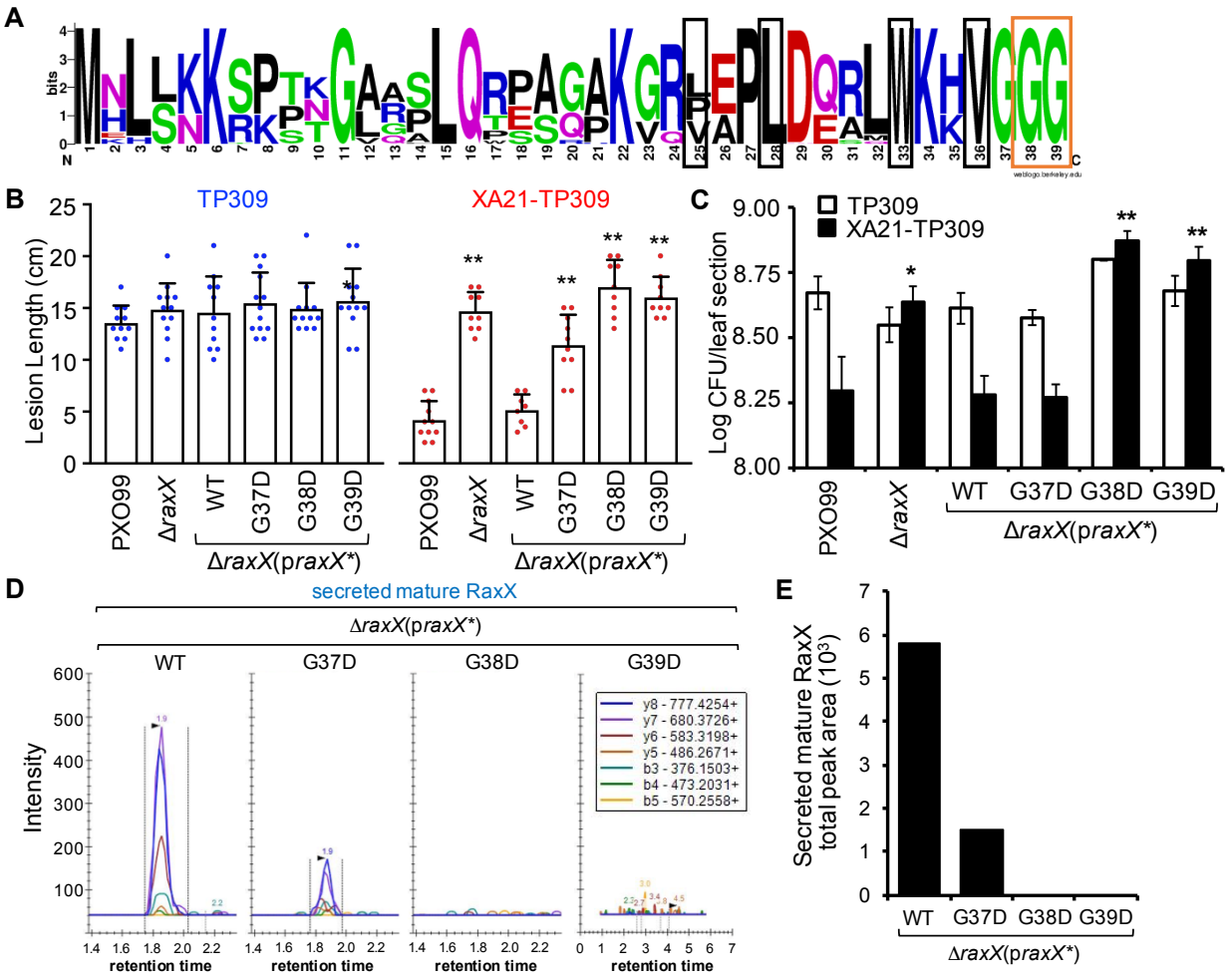
A
bits
N
C
B
TP309
XA21-TP309
Lesion Length (cm)
PXO99
ΔraxX
WT
G37D
G38D
G39D
ΔraxX(praxX*)
C
TP309
XA21-TP309
Log CFU/leaf section
D
secreted mature RaxX
ΔraxX(praxX*)
WT
G37D
G38D
G39D
Intensity
retention time
y8 - 777.4254+
y7 - 680.3726+
y6 - 583.3198+
y5 - 486.2671+
b3 - 376.1503+
b4 - 473.2031+
b5 - 570.2558+
E
Secreted mature RaxX total peak area (10³)

Figure 7